IOP Publishing Nanotechnology
Nanotechnology 25 (2014) 445103 (11pp) doi:10.1088/0957-4484/25/44/445103

A new magnetic resonance imaging contrast agent loaded into poly(lacide-co-glycolide) nanoparticles for long-term detection of tumors

G Rigaux[1,2], V G Roullin[2,8], C Cadiou[1], C Portefaix[3], L Van Gulick[4], G Bœuf[2,5], M C Andry[2], C Hoeffel[3], L Vander Elst[6,7], S Laurent[6], R Muller[6,7], M Molinari[5] and F Chuburu[1]

[1] Institut de Chimie Moléculaire de Reims, CNRS UMR 7312, UFR des Sciences Exactes et Naturelles, Bâtiment 18-Europol'Agro, BP1039, F-51687 Reims Cedex 2, France
[2] Institut de Chimie Moléculaire de Reims, CNRS UMR 7312, UFR Pharmacie Reims, 51 rue Cognacq-Jay, F-51100 Reims, France
[3] Service de radiologie, CHU de Reims-Hôpital Maison Blanche F-51092 Reims Cedex, France.
[4] Laboratoire de pharmacologie, CNRS 3481 MEDyC, UFR Pharmacie F-51095 Reims Cedex, France
[5] Laboratoire de Recherche en Nanosciences—EA 4682, Université de Reims Champagne-Ardenne URCA, F-51685 Reims Cedex 2, France
[6] Laboratoire de RMN et d'imagerie moléculaire, Université de Mons, B-7000 Mons, Belgique
[7] Center for Microscopy and Molecular Imaging, Rue Adrienne Bolland 8, B-6041 Charleroi (Belgium)

E-mail: vg.roullin@umontreal.ca and francoise.chuburu@univ-reims.fr

Received 22 June 2014, revised 8 September 2014
Accepted for publication 11 September 2014
Published 17 October 2014

Abstract

The incorporation of a lipophilic Gd chelate (GdDO3A-C_{12}) in biocompatible PLGA poly(D, L-lactide-co-glycolide) nanoparticles was explored as an approach to increase the relaxivity of contrast agents for magnetic resonance imaging. By nanoprecipitation, it was possible to obtain PEGylated gadolinium nanoparticles (mean diameter of 155 nm) with high Gd loading (1.1×10^4 Gd centers per nanoparticle). The corresponding GdDO3AC_{12} ⊂ NPs nanoparticles exhibited an enhanced relaxivity (up to sixfold greater than DOTAREM® at 40 MHz) because the nanoparticle framework constrained the lipophilic Gd chelate motion and favorably impacted the Gd chelate rotational correlation time. T_1-weighted imaging at 3 T on phantoms showed enhanced contrast for the GdDO3AC_{12} ⊂ NPs. Importantly, Gd chelate leakage was almost nonexistent, which suggested that these GdDO3AC_{12} ⊂ NPs could be useful for long-term MRI detection.

Keywords: MRI contrast agents, gadolinium complex, PLGA nanoparticles, biocompatible materials

(Some figures may appear in colour only in the online journal)

Introduction

Magnetic resonance imaging (MRI) is a routinely used diagnostic tool in both clinical and research fields. It is non-invasive, delivers no radiation burden and readily yields anatomical information, thanks to its excellent spatial resolution [1]. The physical principles of MRI rely on the

[8] Present address: Pharmaceutical Nanotechnology Laboratory, Faculty of Pharmacy, Université de Montréal, CP6128, succursale Centre-ville, Montreal QC, H3C 3J7, Canada.

relaxation of water protons, which depends on the magnetic fields (the strong static magnetic field B_0 and the radio-frequency field), on the pulse sequence and on the heterogeneous distribution and environment of water in the organism [2]. However, MRI suffers from low sensitivity, and the contrast often has to be amplified by administering contrast-enhancing agents (CAs). Among MRI contrast agents, the most currently used contrast agents are T_1-CAs. They are constituted of paramagnetic complexes of metal ions such as gadolinium (GdCAs). These substances catalytically increase the longitudinal relaxation rate ($1/T_1$) of water protons in the tissues. This effect is translated into an increased MRI signal intensity for positive contrast agents. Commercially available Gd-based contrast agents are hydrophilic substances characterized by short distribution and elimination half-lives. Whatever the GdCA, the distribution occurs in minutes (less than 15 min), and the elimination half-life is around 1.5 h in patients with normal renal function [3].

Therefore, if a serial set of images is needed in a short period of time, multiple injections of high doses are required. Until recently, all GdCAs were considered safe. Unfortunately, it has been demonstrated that some of them may trigger the development of nephrogenic systemic fibrosis (NSF) in patients with renal failure [4]. Consequently, there is a need to develop GdCAs with a longer residence time. In this context, the association of metal complexes to nanosized systems represent a current option [5, 6]. Many systems have therefore been developed including dendrimers [7], natural [8] or modified natural nanoparticles [5], auto-assembled systems [9], metal-organic frameworks [10], fullerenes [11] inorganic nanoparticles [12] and nanogels [13, 14].

However, the biocompatibility of these objects is a crucial factor whenever *in vivo* applications are implied. In this respect, polymeric biocompatible nanoparticles (NPs) are ideal candidates for the vectorization of contrast agents. Among them, aliphatic polyesters like poly(D, L-lactide-co-glycolide) PLGA have generated tremendous interest due to their excellent biocompatibility and biodegradability [15–17]. Since GdCAs are usually hydrophilic chelates, the challenge was to achieve high Gd loadings inside PLGA NPs; indeed, hydrophilic substances present a very low affinity for this kind of polymer matrix [17, 18]. To achieve this goal, a chemical modulation of GdDOTA (GdCA of DOTAREM®), which is a well-known and low-risk CA, was undertaken. A hydrophobic C_{12} side-chain was grafted on the GdDOTA backbone in order to promote Gd contrast agent encapsulation inside PLGA NPs. Herein, the synthesis of the corresponding $GdDO3AC_{12}$ complex and its incorporation inside PLGA nanoparticles are reported. The ability of the corresponding Gd-loaded NPs to act as an MRI contrast agent was evaluated by means of relaxometric measurements and 3 T MRI images. Finally, nanosuspension stability and cell viability assays were performed to evaluate the potential use of these Gd-loaded NPs for parenteral administration.

Materials and methods

General

All chemicals were used as received without further purification. The poly(lactide-co-glycolide) RG503H (PLGA, 50:50 lactide/glycolide) was purchased from Boehringer, Ingelheim. The poloxamer 188 (Pluronic® F-68, polyethyleneglycol-co-polypropyleneglycol-co-polyethyleneglycol), glycofurol (tetrahydrofurfuryl polyethyleneglycol) and N,N-dimethylacetamide (DMA) were obtained from Sigma-Aldrich, France. The water was from Versol® (Aguettant laboratory, France). The β-cyclodextrin (Kleptose®) was purchased from Roquette. The human serum albumin (HSA) was purchased from Laboratoire Français du Fractionnement et des Biotechnologies. The cyclen (1,4,7,10-tetraazacyclododecane; 98%) was purchased from Strem Chemical, USA. The *Tert*-butylbromoacetate ($BrCH_2CO_2t$-Bu, 98%), 1-bromododecane ($C_{12}H_{25}Br$, 98%) and trifluoroacetic acid (TFA, 99%) were obtained from Alfa Aesar, France. The sodium acetate (NaOAc) and sodium hydrogenocarbonate were obtained from R.P Normapur, France. The cesium carbonate (Cs_2CO_3) came from Fluka, France. The Dulbecco's Modified Eagle's Medium Gibco® was purchased from Life Technologies, France.

The ^1H and ^{13}C NMR experiments were performed on a Bruker 250 DPX Spectrometer at 250 MHz. The chemical shifts were given as δ values with reference to $CDCl_3$ or D_2O as an internal standard. The coupling constants are in Hz. The mass spectra were obtained by using a Micromass ESI-Q-TOF with a negative ionisation spectrophotometer in methanol and a Micromass Waters Maldi-TOF with a positive ionisation apparatus (dithranol matrix 10 mg ml^{-1} in MeOH). The elemental analyses were performed by a Flash EA 1112 series apparatus.

Synthesis of the $GdDO3AC_{12}$ complex

Synthesis of DO3A(t-Bu)$_3$ (1,4,7-Tris(tert-butoxycarbonylmethyl)-1,4,7,10-tetraazacyclododecane) 1. The synthesis is adapted from previously published works by Raghunand *et al* [19]. Briefly, a solution of $BrCH_2CO_2t$-Bu (35.3 mmol; 3 eq) in DMA (10 mL) was added dropwise to a mixture of cyclen (11.6 mmol) and NaOAc (34.8 mmol). The reaction was maintained during six days at 0 °C; afterward, $NaHCO_3$ was added to provoke ester **1** precipitation. The solid was isolated by filtration, washed thoroughly with water and ether and dried. Ester **1** was finally obtained as a white powder (8.2 mmol, yield = 70%).

^1H NMR (250 MHz, $CDCl_3$) δ(ppm) 1.46 (s, 27H, *t*-Bu); 2.90–2.93 (m, 16H, cyclen); 3.30–3.39 (m, 6H, CH_2CO_2t-Bu); 10.09 (s, 2H, NH_2).

^{13}C NMR (250 MHz, $CDCl_3$) δ(ppm) 28.6; 47.9; 49.1; 49.6; 51.6; 51.7; 58.6; 82.1; 82.2; 170.0; 171.0.

Synthesis of DO3A(t-Bu)$_3$C$_{12}$ 2. Cs_2CO_3 (2.5 mmol; 3 eq) was added to a solution of **1** (0.4 mmol) in dry acetonitrile (20 mL). The solution was left under stirring under an argon flow overnight. Then, $C_{12}H_{25}Br$ (0.5 mmol, 1.2 eq) was

added. The mixture was left at room temperature for five days before being filtered. The filtrate was evaporated to dryness under reduced pressure. The oily residue was dissolved in dichloromethane (3 × 100 mL) and filtered again. The filtrate was concentrated, and the ether addition provoked the product precipitation. After drying under reduced pressure, DO3A(t-Bu)$_3$C$_{12}$ **2** was obtained (0.4 mmol, yield = 93%).

^{1}H NMR (250 MHz, $CDCl_3$) δ(ppm) 0.81 (t, 3H, J = 6.47Hz); 1.10-1.31 (m, 22H); 1.47 (s, 27H, *t*-Bu); 2.2-2.85 (m, 16H); 3.18 (d, 6H, J = 10.75 Hz).

^{13}C NMR (250 MHz, $CDCl_3$) δ(ppm) 14.5; 15.6; 23.0; 27.9; 28.6; 29.7; 30.0; 32.2; 52.2; 52.3; 52.4; 52.8; 56.6; 57.0; 66.1; 80.9; 171.4.

Deprotection of ***2****: synthesis of the DO3AC$_{12}$ ligand* ***3****.* TFA (10 mL) was added dropwise to a solution of **2** (0.4 mmol) in dichloromethane (2 mL). The mixture was stirred during 3 days at room temperature. An oily product was obtained by evaporation under reduced pressure. Ether (40 mL) was added to precipitate the ligand **3** as a brown solid, which was collected by filtration (0.3 mmol, yield = 74%).

^{1}H NMR (250 MHz, D_2O) δ(ppm) 0.80 (t, 3H, J = 5.00 Hz); 1.21-1.66 (m, 22H); 2.88-4.00 (m, 22H).

^{13}C NMR (250 MHz, D_2O) δ(ppm) 13.6; 22.3; 28.7; 29.2; 29.3; 29.4; 29.5; 31.6; 47.8; 48.2; 49.4; 49.5; 51.4; 53.0; 54.2; 55.6; 168.9; 173.7.

ES/MS m/z calculated for (M–H): [$C_{26}H_{49}N_4O_6$]: 513.7; found 513.2.

IR(KBr, ν: cm^{-1}): ν(CO): 1686.

Synthesis of the GdDO3AC$_{12}$ complex ***4****.* Ligand **3** (1.4 mmol, 1 eq) was dissolved in water (40 mL), and the pH was adjusted to 6 by the addition of 0.1 M NaOH. A solution of $Gd_2(SO_4)_3$ (0.7 mmol, 1 eq) in water (10 mL) was then added dropwise. After every addition, the pH was checked and adjusted as needed. When the addition was complete, complex **4** precipitated as a white powder, which was collected, filtered and dried under a vacuum (0.88 mmol, yield = 63%).

Maldi-TOF LD$^+$ calculated for (M+H): [$C_{26}H_{47}GdN_4O_6$-H]$^+$: 670.3; found: 670.4

IR(KBr, ν: cm^{-1}): ν(CO): 1577.

Nanoparticle preparation

The nanoparticles were synthesized using a modified nanoprecipitation method [20]. Briefly, 50 mg of PLGA (1% w/v) and 50 mg Pluronic® F68 (1% w/v) were dissolved in glycofurol (5 mL) in the presence of GdDO3AC$_{12}$. Then, this organic solution was poured at a constant flow rate (0.2 mL min^{-1}) under moderate magnetic stirring into 75 mL of an aqueous phase containing 4.4 mM β-cyclodextrin and 0.01% w/v Pluronic® F68. The nanoparticles were spontaneously formed upon glycofurol diffusion into the aqueous phase. Potential aggregates were removed by centrifugation (3800 rpm for 5 min, RT).

The raw nanosuspension was then purified by dialysis, followed (as needed) by tangential flow filtration. Dialysis was performed by introducing the raw nanosuspensions (typically 10 mL) into a dialysis membrane (Spectrum, Spectrapor® 6.0 MWCO 25 kDa). The nanosuspensions were dialyzed three consecutive times at room temperature against 1 L of sterile water for 10 h. In order to improve the separation from free complexes and to concentrate the nanoparticles, tangential flow filtration was carried out using a MicroKros® apparatus (Spectrum, France) equipped with a modified polysulfone (mPES) hollow fiber with a cut-off of 0.1 μm and a specific surface of 10 cm^2. Typical concentration factors were in the 5–10 fold range.

Determination of encapsulation efficiencies

Gadolinium loading into nanoparticles was determined on raw and purified nanoparticle suspensions by ICP-OES, as previously described [21]. The Gd-complex entrapment efficiency (EE, %) and drug loading (DL, % w/w) were calculated by equations (1) and (2), respectively.

$$EE\% = \frac{Gd\ mass\ in\ nanoparticles}{Gd\ mass\ introduced\ in\ the\ synthesis} \times 100 \quad (1)$$

$$DLE\% = \frac{Gd\ mass\ in\ nanoparticles}{total\ mass\ of\ recovered\ nanoparticles} \times 100 \quad (2)$$

Particle size analysis and ζ-potential measurements

Dynamic light scattering (DLS) was used for the measurement of average hydrodynamic diameters (D_h) and polydispersity indexes (PdI) using a Malvern Zetasizer Nano-ZS (Malvern Instruments, UK). Each sample was analyzed in triplicate (20 °C, scattering angle of 173°).

The Zeta potential (ζ-potential or ZP) data were collected through electrophoretic light scattering (ELS, 20 °C, 150 V), in triplicate for each sample (Malvern Zetasizer Nano-ZS, Malvern Instruments, UK). The instrument performance was checked with a Malvern –42 mV standard before each analysis cycle.

Water was taken as the dispersant medium for both the DLS and ELS measurements.

The percentage of (size, PdI or ZP) the variations according to time was calculated from values at time = 0 (synthesis day), which is defined as 100% for the size and for the PdI and as 0% for the ζ-potential.

Morphological studies

The shape and surface morphology of Gd-loaded NPs were investigated by atomic force microscopy (AFM) (Catalyst, BrükerNano), and local infrared absorption spectra were acquired on single NPs (empty or loaded) using the NanoIR AFM from Anasys. Samples for AFM imaging were prepared by placing a drop of the purified nanosuspension on a freshly cleaved mica sheet, and the morphological experiments were performed in fluid to keep the NP integrity. The images were

acquired in a tapping mode, and the parameters were set to avoid strong interactions between the tip and the soft sample and thus avoid a possible deformation of the NPs. A silicon nitride tip with a spring constant of 0.4 N m^{-1} was used for the topographical images. AFM images were generated with a scan rate of 0.5 Hz and with 512 lines per image. The experiments were performed at constant room temperature. During the scans, feedback gains were increased to the value just below the point at which the feedback started to oscillate. The images were processed only by flattening to remove background slopes.

To perform local IR absorption measurements, the samples were dried after placing a drop of the purified suspension on a ZnSe prism. Thanks to a low density of NPs, the IR absorption spectra were performed on a tenth of the NPs so as to present a good statistic of the measurements.

In vitro stability and release studies

In order to investigate the nanosuspension stability, purified nanosuspensions ($n=9$) were aliquoted and placed at three different thermal conditions (8 °C, 20 °C, 37 °C). At pre-fixed endpoints, the aliquots were allowed to re-adjust to room temperature, and DLS/ELS measurements were undertaken as previously described.

For the *in vitro* release study, purified $GdDO3AC_{12}$-loaded nanoparticles ($n=3$ batches) were dispersed in a sodium phosphate buffer (pH 7.4, 40 mL). The release medium was supplemented with 5% w/v as a natural solubility enhancer in order to maintain sink conditions for the lipophilic $GdDO3AC_{12}$. All of the samples were kept at 37 °C under magnetic stirring. At various pre-determined endpoints, 40 mL aliquots were centrifuged (23 200 g, 1 h 15, 4 °C). The pellets were consecutively separated from the supernatants and treated as previously described.

In vitro cytotoxicity studies

The murine C6 glioma cell line and the primary murine fibroblast cells were used in this study. About 5×10^3 cells per well were seeded in 96-well plates and grown in Dulbecco's Modified Eagle's Medium, enriched with 10% FCS. Thereafter, the cells were incubated with various concentrations of $GdDO3AC_{12}$-loaded NPs and equivalent NP concentrations of unloaded NPs. The control cells were left untreated. The cells were incubated with various treatments for 48 h at 37 °C, 5% CO_2. After carefully removing the medium and rinsing the cells with PBS, cell survival was determined by a MTT assay [22]. The cytotoxicity was expressed as percentage of controls (untreated cells) by visible spectrophotometry (Victor3V) at 560 nm (Perkin Elmer 1420 Multilabel Counter; software: Wallac 1420 Manager).

Relaxometry and MRI studies

Longitudinal (T_1) and transverse (T_2) relaxation time measurements were performed using Bruker Minispec mq at 20, 40 and 60 MHz (0.5–1.5 T), 37 °C. T_1 and T_2 were obtained from a mono-exponential fit of the signal intensities as a function of recovery time or echo time, respectively. The diamagnetic contribution was determined by recording paramagnetic longitudinal and transversal times from the unloaded NP and media without a Gd-complex (water and β-cyclodextrin) at the same concentrations as the Gd-loaded samples. The relaxivity, r_1 and r_2, were determined by linear fits of $1/T_1$ and $1/T_2$ versus the Gd concentration after subtraction of the diamagnetic contribution. Each sample was analyzed by ICP-OES to obtain the exact Gd concentration.

The ^1H NMRD profile of a $GdDO3AC_{12}$ solution (containing 4 mM β-cyclodextrin) was recorded on a Stelar Spinmaster FFC Fast Field Cycling NMR Relaxometer (Stelar, Mede, Pavia, Italy) over a range of magnetic fields extending from 0.24 mT to 0.7 T and corresponding to ^1H Larmor frequencies from 0.01 to 30 MHz using 0.6 mL samples in 10 mm OD tubes. The temperature was kept constant at 37 °C. Additional relaxation rates at 60 and 300 MHz were obtained with a Bruker Minispec mq60 spectrometer and a Bruker Avance, respectively (Bruker, Karlsruhe, Germany). The diamagnetic contribution of β-cyclodextrin was measured and subtracted from the observed relaxation rates of the Gd-loaded nanoparticles. The molecular parameters were extracted from the fitting of the NMRD profile using the classical inner sphere and outer sphere theories. For the $GdDO3AC_{12}$, the distance between the water protons of the first coordination sphere and the paramagnetic center was fixed to 0.31 nm, and the distance of the closest approach was fixed to 0.36 nm, whereas the diffusion constant was set to 3×10^{-9} m^2s^{-1}. The water residence time in the first coordination sphere τ_M was fixed at 50 ns, and two water molecules were considered for the complex. In these conditions, the optimization led $GdDO3AC_{12}$ to a rotational correlation time τ_R of 127.0 ± 1.8 ps to an electronic relaxation time at a very low field τ_{SO} of 65.6 ± 0.8 ps and to a correlation time modulating the electronic relaxation τ_V of 25.8 ± 1.1 ps. A similar fitting was performed for GdDOTA as a reference. The fixed parameters were the same, except for the water residence time in the first coordination sphere ($\tau_M = 120$ ns) and the number of water molecules for the complex ($q=1$), and the diffusion constant was set to 3.3×10^{-9} m^2s^{-1}. In these conditions, the optimization led GdDOTA to a rotational correlation time τ_R of 47.1 ± 1.5 ps to an electronic relaxation time at a very low field τ_{SO} of 576 ± 112 ps and to a correlation time modulating the electronic relaxation τ_V of 4.8 ± 1.3 ps.

MR imaging of the nanoparticle suspensions were performed using a 3.0 T MRI device (Achieva, Philips Medical Systems, the Netherlands) with a Sense head 8 channels coil. The T_1-weighted images were obtained with an axial spin echo T_1 sequence ($TR = 160$ ms, $TE = 8$ ms, $FOV = 170 \times 170$ mm, matrix $= 192 \times 192$, slice thickness $= 2$ mm, excitation number $= 1$). The T_2-weighted images were obtained with an axial turbo spin echo T_2 (TSE multishot) sequence ($TR = 5000$ ms, $TE = 80$ ms, $FOV = 100 \times 100$ mm, matrix $= 256 \times 256$, slice thickness $= 2$ mm, excitation number $= 1$).

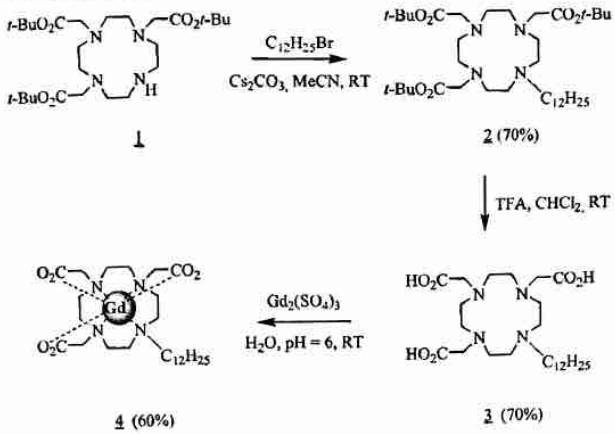

Scheme 1. Synthesis of $GdDO3AC_{12}$.

Results and discussion

$GdDO3AC_{12}$ synthesis

$DO3AC_{12}$ (Ligand **3**, scheme 1) was readily obtained through a three-step procedure.

In the first step, ester **1** was prepared from commercially available cyclen by reaction with 3 equivalents of *tert*-butyl bromoacetate and sodium acetate in *N, N*-dimethylacetamide, according to a published procedure [19]. In the second step, *N*-alkylation of **1** with 1-bromododecane with cesium carbonate as a base gave ligand **2** in a 70% yield. In the third step, the removal of *tert*-butyl groups was carried out with trifluoroacetic acid, leading to the expected fully deprotected tricarboxylic acid **3** in a 70% yield. Ligand **3** was then reacted at room temperature with $Gd_2(SO_4)_3$ at pH 6 to give the corresponding Gd(III) complex **4** in a 60% yield. This complex was freely soluble in alcohols and, due to the C_{12} side chain, was sparingly soluble in water. The structure of compounds **1–3** were characterized by ^1H and ^{13}C NMR spectroscopies and mass spectrometry. The $GdDO3AC_{12}$ gave an appropriate mass in the MS analysis. The IR analysis of the ligand **3** (ν_{CO}: 1686 cm^{-1}) and complex **4** (ν_{CO}: 1577 cm^{-1}) carboxylic acid vibrators indicated a weakening of the C=O wavelength upon complexation, which is attributable to the involvement of the acid functions to the Gd complexation.

Physicochemical and morphological characteristics of $GdDO3AC_{12}$-loaded NPs

The biodegradable $GdDO3AC_{12}$-loaded nanoparticles were synthesized from FDA-approved, pharmaceutical-grade PLGA through the simple and easily scalable nanoprecipitation process [20]. The procedure used herein was based on previous works using exclusively nontoxic ingredients [23, 24]. Nonetheless, it was adapted to address the poor aqueous solubility of $GdDO3AC_{12}$. Indeed, the non-encapsulated fraction of $GdDO3AC_{12}$ was able to induce NP instability and therefore induce flocculation within minutes, whatever the Gd-complex concentration (data not shown). This drawback was countered by using β-cyclodextrin in the external aqueous phase. Because this cyclic molecule presents a hydrophobic cavity surrounded by a hydrophilic outer surface, it is able to form complexes with hydrophobic compounds. Thus, the solubility and bioavailability of such compounds are enhanced, which is highly attractive [25]. Alpha-, beta- and gamma-cyclodextrins are included in the FDA Inactive Ingredients Database [26]. In our case, it is believed that the hydrophobic C_{12} side-chain of $GdDO3AC_{12}$ was able to insert in the hydrophobic pocket of β-cyclodextrin, thus rendering the molecule soluble in aqueous solutions. This hypothesis was supported by the fact that the sparingly water-soluble $GdDO3AC_{12}$ turned increasingly water-soluble, as the β-cyclodextrin concentration was raised in the aqueous medium. Finally, a 4.4 mM solution was chosen as the best concentration to enable NP formation and stability. This value is far above the 1:1 ratio usually reported for cyclodextrins [27] but is explainable by the presence of various compounds able to compete in the diffusing aqueous phase (tensioactive and solvent molecules, for instance).

Table 1. Physicochemical data of unloaded and $GdDO3AC_{12}$-loaded NPs ($n = 9$).

	Unloaded NPs		$GdDO3AC_{12}$-loaded NPs	
	Raw NPs	Dialyzed NPs	Raw NPs	Dialyzed NPs
D_h (nm)	127 ± 20	111 ± 18	177 ± 15	155 ± 29
ζ (mV)	−17 ± 2	−30 ± 3	−13 ± 1	−27 ± 6
EE (%)	—	—	30 ± 4	10 ± 7
DLE (%)	—	—	1.6 ± 0.2	0.4 ± 0.2
Y_{Gd}	—	—	5×10^4	1.1×10^4

The physicochemical characteristics of the $GdDO3AC_{12}$-NP are presented in table 1.

All nanoparticle suspensions displayed monodisperse size distributions (PdI < 0.15), with average hydrodynamic diameters between 120 and 180 nm. The Gd-loading increased the mean hydrodynamic diameter but was within acceptable range for IV administration and to forestall rapid renal clearance [28]. Whether purified or not, the particles showed a negative surface charge. This property is considered a conclusive point to ensure long-term nanosuspension stability [29]. Nevertheless, the ZP is superior to what is expected for PLGA-based NPs prepared in the same conditions in the absence of Pluronic® P188 (~ −50 mV [30]). This characteristic demonstrates that a partial PEG-coating occurred due to the co-precipitation of PLGA and Pluronic® P188 [31]. Therefore, the orientation of the PEG segments to the NP-water interface allowed partial masking of the carboxylic end-groups at the PLGA NP surface. This participated to the formation of a hydrophilic PEG corona [32], which contributed to render those NPs less vulnerable to opsonization [33].

AFM imaging allowed us to confirm the spherical shape and size range characteristics of the designed NPs. Figure 1(a) shows typical $GdDO3AC_{12}$-loaded PLGA NPs.

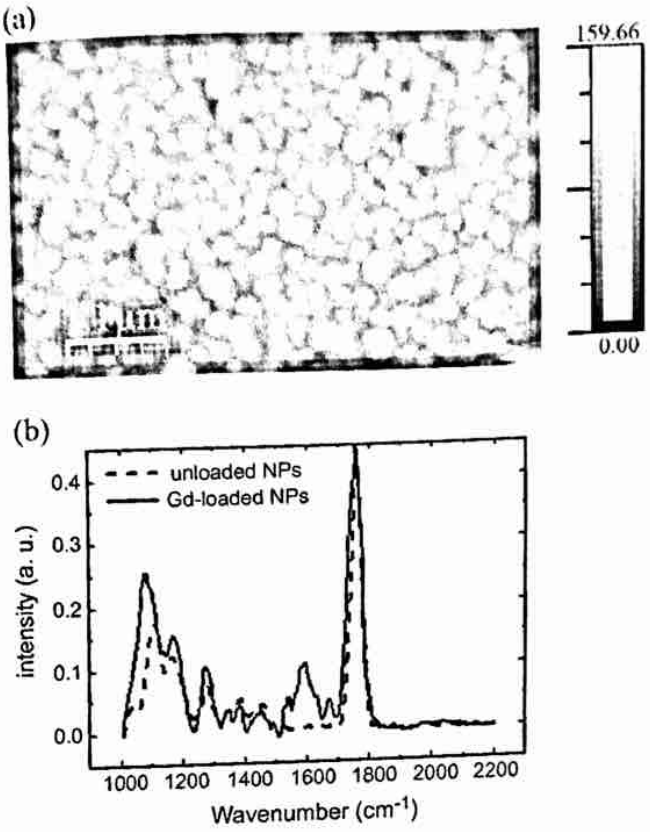

Figure 1. (a) Typical AFM picture of $GdDO3AC_{12}$-loaded PLGA NPs obtained under a liquid condition. (b) Local IR absorption spectra of $GdDO3AC_{12}$-loaded PLGA NPs (red line) and the corresponding unloaded NPs (black line).

The presence of the Gd-complex within the NPs was checked by the local AFM-IR spectrum of Gd-loaded NPs (figure 1(b)). By comparison, with unloaded NPs, an additional broad band centered at 1570 cm^{-1} was observed for the Gd-loaded NPs. This wavelength, similar to the one attributed to the COOH vibrators in the $GdDO3AC_{12}$ complex, demonstrated the presence of the complex within the NPs.

This point was later confirmed by the direct assessment of Gd content by ICP-OES (table 1). Due to its better affinity for PLGA, the drug encapsulation and loading efficiencies of lipophilic $GdDO3AC_{12}$ were largely increased compared to previous attempts with GdDOTA [34]. Indeed, the Gd amount per NP was comparable with similar [15, 35, 36] or even more hydrophilic nanosystems [37–39]. This is an interesting result, as it was obtained through the simple hydrophobic interaction within the polymer matrix. This led to an average number of 1.1×10^4 Gd chelates per NP after dialysis, i.e. a mean value of 1.12 μg Gd per mg NP.

In vitro stability and release results

One of the numerous pitfalls of polymeric NP suspensions is their potential lack of stability with regard to long-term preservation and environmental conditions. This instability may be related to chemical degradation, such as polymer hydrolysis [40] or to colloidal instability, i.e. a propensity to form flocculates that evolve into aggregates [41]. Therefore, the biological fate of drug-loaded nanosuspensions will be closely related to their global stability [42]. In our case, the chemical stability of this type of formulation had already been examined [23]. In this study, the colloidal stability was assessed as a function of size and size distribution evolution upon time, as well as changes in the NP surface charges, for dialyzed NPs. These parameters were selected as they reflect the changes that may occur during an aggregation process. Indeed, molecular adsorption at the NP surface (objectified by ZP changes) can create surface inhomogeneities that will in turn favor NP flocculation (a PdI increase) and then aggregation (a mean hydrodynamic diameter increase) [43]. Three different temperature conditions were set: 8 °C for refrigerated preservation, 20 °C for room temperature conditions and 37 °C to correspond to body (administration) temperature. Figure 2 illustrates the observed changes.

A ± 5% tolerance window was selected for the size evolution to discriminate between the tested conditions. This percentage was set arbitrarily in absence of FDA-EMA guidelines specifically aimed at NP stability [44]; nevertheless, this value is generally chosen for more conventional pharmaceutical formulations.

Globally, the nanosuspensions were stable and monodispersed during two to three weeks, except at 37 °C, when they became unstable after one week, as stated by the size and ZP changes (figures 2(a) and (c)). The best condition to preserve purified NP suspensions was found to be 8 °C and was therefore adopted for further experiments. These results were in agreement with those obtained by Zweers *et al*, who demonstrated that *in vitro* degradation of the PLGA nanoparticles in PBS occurred slowly for two weeks at 37 °C [45]. This process will be even slower at a lower temperature. In this context, our DLS experiments correlated perfectly with those previous findings.

The *in vitro* $GdDO3AC_{12}$ release profile from the synthesized PLGA nanoparticles was performed in a phosphate buffer (pH 7.4, 37 °C) in the presence of 5% HSA (figure 3).

Due to poor water solubility, maintaining sink conditions for the $GdDO3AC_{12}$ was not experimentally possible. Hence, the addition of 5% HSA (within the physiological plasmatic concentration range) allowed us to solve this limitation, as already reported [46]. Indeed, preliminary experiments showed that the $GdDO3AC_{12}$ turned highly soluble and rapidly dissolved in the presence of 2 to 10% HSA (data not shown). It was hypothesized that the HSA hydrophobic pocket could interact with the C_{12} hydrophobic tail of free $GdDO3AC_{12}$, as it acts to destabilize liposomes, for instance [47]. Another interesting observation was that no flocculation/aggregation occurred when the $GdDO3AC_{12}$-loaded NPs were dispersed in this highly-concentrated salt/protein solution.

A monophasic release profile characterized by near-zero order release kinetics was monitored for 16 days (figure 3). Based on these data, less than 1% of the $GdDO3AC_{12}$ was released each day. This result highlighted the development of strong interactions between the $GdDO3AC_{12}$ and the

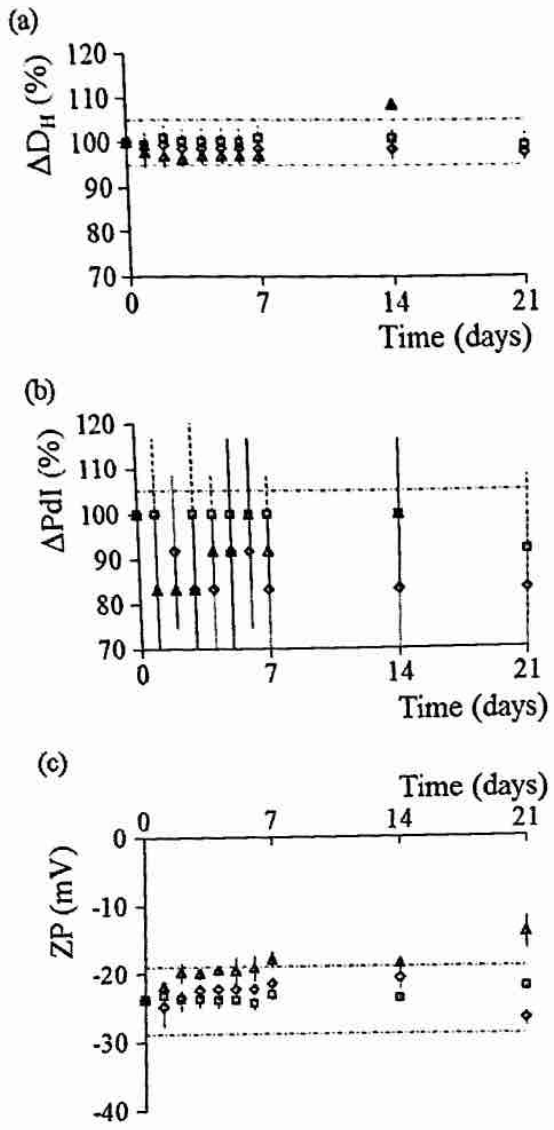

Figure 2. Variations of the (a) average hydrodynamic diameter, (b) PdI values and (c) Zeta potential as a function of time for the dialyzed Gd-loaded NPs: $T = 8$ °C (squares), room temperature (diamonds) and 37 °C (triangles). The dotted red lines set the limits for the acceptable variations.

hydrophobic PLGA core of the loaded NPs. Usually, polyester-based nanodevices display a burst effect due to the rapid release of surface-associated drug molecules [46, 48, 49]. In our study, however, its absence signaled that almost no $GdDO3AC_{12}$ molecules were weakly bound to the NP's surface. Therefore, the very slow release kinetics observed in our case demonstrated the suitability of the nanocarrier design for the intended extended entrapment of this new Gd derivative.

Cytotoxicity studies

A preliminary stage to determine how nanoparticles will react after *in vivo* administration was performed by testing cell viability when in contact with the nanoparticles. For that, an

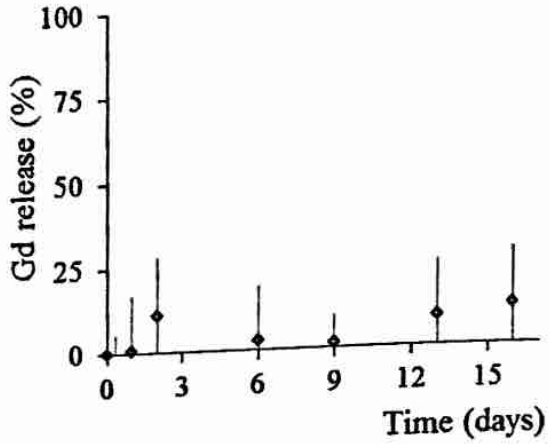

Figure 3. Release patterns of purified $GdDO3AC_{12}$-loaded PLGA nanoparticles as a function of time in a phosphate buffer, pH = 7.4, 5% HSA, 37 °C.

MTT colorimetric assay was used to quantify cell survival [50]. The mitochondrial activity can be measured using tetrazolium salts to be enzymatically cleaved, based on the fact that only active mitochondria will be able to generate the coloured substrate [22]. In this study, two different cell lines were used. The C6 glioma cell line (ATCC® CCL-107) was selected as a model tumor cell line. It is a fast-growing cell line and henceforth prone to markedly and rapidly react in the presence of toxic compounds. Furthermore, it shows no significant expression of the multidrug resistance protein, Pgp [51]. This means that the detoxification processes will be low in the case of toxic exposure. Primary fibroblasts from rat skin were used as normal, unmodified cells. Although they are lower-growing cells, they are generally considered pertinent material to study phenomena such as terminal differentiation, aging, apoptosis and transformation [52].

Cell survival was explored for Gd concentrations ranging from 0.02 to 5 μM and hence from 2.5 to 633 $\mu g.mL^{-1}$ for the corresponding dilutions of unloaded (blank) nanoparticles and for the 48 h incubations (figure 4).

Both the blank and Gd-loaded NPs were prepared and purified through a sterile process. Neither the blank nor the $GdDO3AC_{12}$-loaded NPs showed any toxicity in the presence of the primary fibroblasts (figure 4(a)). Nevertheless, both the blank and $GdDO3AC_{12}$-loaded NPs were slightly toxic to C6 glioma cells at concentrations over 2 μM (figure 4(b)). However, the IC_{50} of both formulations could not be reached in the investigated concentration ranges. Previous studies with blank NPs obtained through similar synthesis protocols [23] led us to assume that residual β-cyclodextrin, the only additional ingredient, was responsible for such toxicity at higher concentrations. Indeed, the cellular toxicity of β-cyclodextrin is known to be related to the tested cell line and can be modulated by the appropriate use of its hydroxypropyl derivative [53]. Further investigations would be needed to ensure hemocompatibility and a low toxicity profile, as these preliminary results suggest.

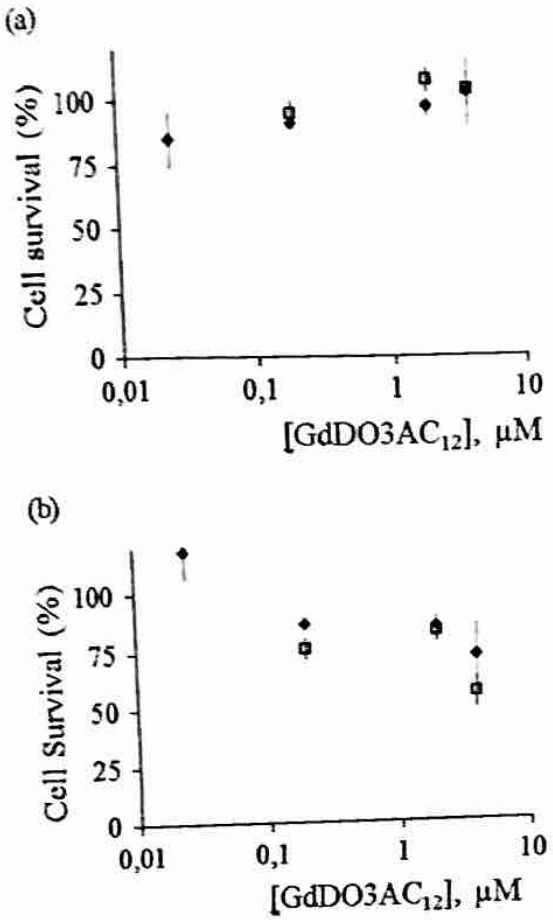

Figure 4. Percentage of cell survival in the presence of $GdDO3AC_{12}$-loaded NPs (black diamonds) and unloaded NPs (open squares) as a function of increasing concentrations (μM) on (a) fibroblasts and (b) C6 cells. The results are obtained after 48 h of incubation.

Relaxivity assessments and MRI studies

Since the $GdDO3AC_{12}$ was sparingly soluble in water, its water proton relaxation rate was determined in the presence of β-cyclodextrin (table 2). In these conditions, the variation of $(1/T_{1,2})$ with the $GdDO3AC_{12}$ concentration was linear (a concentration range of 0.1–0.15 mM), which indicated that the lipophilic complex self-organization was avoided in these conditions [54].

As expected, since the enhancement of the gadolinium complex molecular weight would slow its molecular tumbling motion, the $GdDO3AC_{12}$ exhibited higher relaxivity than the DOTAREM® by threefold at 40 MHz. This enhancement could also be due to the presence in the solution of β-cyclodextrin and the probable formation of $GdDO3AC_{12}/\beta$-cyclodextrin inclusion adducts [55]. This was supported by the shape of the ^{1}H NMRD profile of $GdDO3AC_{12}$ in the range of 20–60 MHz (figure 5), which exhibited a hump in relaxivity typical for Gd contrast agents with a restricted rotational motion [55]. This profile was analyzed using the classical inner sphere and outer sphere theories, which led to a rotational correlation time τ_R of 127.0 ± 1.8 ps, i.e. almost threefold higher than the τ_R of GdDOTA (47.1 ± 1.5 ps).

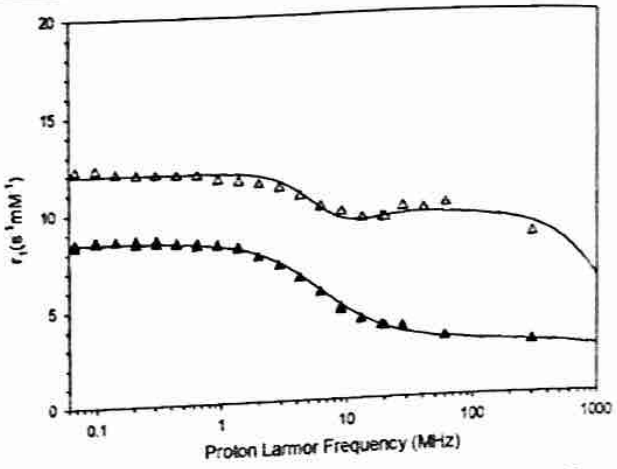

Figure 5. NMRD relaxivity profiles at 37 °C of the $GdDO3AC_{12}$ (open triangles) in the presence of β-cyclodextrine and Gd-DOTA (black triangles). The fitted curves are in the solid lines.

For $GdDO3AC_{12}$-loaded NPs, r_1 relaxivity at 40 MHz (19.4 $mM^{-1}\,s^{-1}$) was twofold greater than for $GdDO3AC_{12}$-β-cyclodextrin adducts (table 2). The incorporation of the gadolinium complex inside of the nanoparticles could account for this additional increase, and this result was comparable to relaxivities measured for gadolinium chelates associated to gold nanoparticles [56], to chitosan nanoparticles grafted with GdDOTA [57] or to nanogels that incorporate GdDOTA [14]. One should therefore notice that for the $GdDO3AC_{12}$-loaded NPs studied herein, the high number of Gd^{3+} per particle (1.1×10^4) allowed a longitudinal relaxivity per nanoparticle larger than 2×10^5 $mM^{-1}\,s^{-1}$ at 40 MHz and 37 °C. This gain in relaxivity not only validated the functionalization strategy of the macrocyclic backbone but also the incorporation of $GdDO3AC_{12}$ within the nanocarriers.

The contrast provided by $GdDO3AC_{12}$-loaded NPs was finally examined by phantom imaging at 3 T on a clinical device (figure 6).

At identical gadolinium concentrations, a better contrast was obtained with the $GdDO3AC_{12}$-loaded NPs compared to the reference contrast agent DOTAREM®. These images corroborated the relaxivities determined at 40 MHz for the Gd-loaded NPs. Moreover, they highlighted the fact that with a smaller dose of gadolinium, a good contrast can be achieved. This strategy, in the context of NSF, could be greatly beneficial to patients.

Conclusion

In this study, the encapsulation of a lipophilic Gd contrast agent, namely $GdDO3AC_{12}$, was carried out within PLGA-based nanoparticles via a fully biocompatible protocol. The lipophilicity of the Gd-complex allowed its encapsulation in yields such that high and stable Gd-loadings were achieved. The relaxivity measurements and MR images clearly demonstrated that the $GdDO3AC_{12}$-loaded nanoparticles exhibited a good ability to enhance T_1-weighted MR images.

Table 2. Relaxivity values for $GdDO3AC_{12}$ (with 0.5% w/v β-cyclodextrin) and $GdDO3AC_{12}$-loaded NPs at 37 °C.

	r_1 ($mM^{-1}s^{-1}$)			r_2 ($mM^{-1}s^{-1}$)		
	20 MHz	40 MHz	60 MHz	20 MHz	40 MHz	60 MHz
$GdDO3AC_{12}$	9.8 ± 0.5	9.7 ± 0.5	9.7 ± 0.5	11.0 ± 0.7	11.7 ± 0.8	10.9 ± 0.7
$GdDO3AC_{12} \subset$ NPs	—	19.4 ± 0.9	—	—	25.8 ± 0.9	—
DOTAREM®	3.5 ± 0.2	3.0 ± 0.2	2.9 ± 0.1	4.2 ± 0.3	3.7 ± 0.2	3.4 ± 0.2

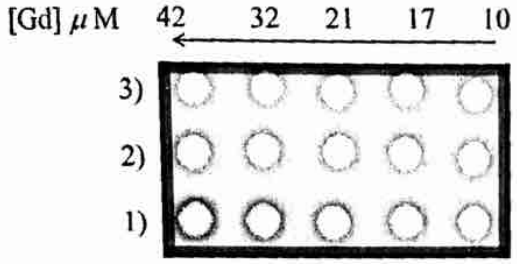

Figure 6. T_1-weighted images of 1) $GdDO3AC_{12}$-loaded NPs, 2) Dotarem® and 3) water as the controls. All of the samples were imaged at 3 T and 37 °C in a standard spin echo (SE) sequence.

This might have been related to the occurrence of high concentrations of entrapped GdCAs and to slow molecular tumbling for the encapsulated complexes. The absence of acute toxicity was also demonstrated in the fibroblasts and C6 cells. Nevertheless, in order to avoid potential Gd leakage from the chelates, the encapsulation of lipophilic DOTA derivatives is currently being examined. Finally, the versatility provided by this approach is also investigated for the development of theranostic agents through the association of contrast agents and active substances such as photosensitizers.

Acknowledgements

G Rigaux thanks the Region Champagne Ardenne for his doctoral fellowship. Authors thank the Region Champagne Ardenne and the EU-program FEDER for their financial support (Project C@nano, NanoMat' and PlAneT platforms). We gratefully acknowledge Dr Sylvain Dukic for the generous gift of the cell lines. The ARC (research contract AUWB-2010—10/15-UMONS-5), the FNRS, ENCITE program, the COST TD1004 (Theranostics imaging and therapy: an action to develop novel nanosized systems for imaging-guided drug delivery), the UIAP VII program, the European Network of Excellence EMIL (European Molecular Imaging Laboratories) program LSCH-2004-503569 and the Center for Microscopy and Molecular Imaging (CMMI, supported by the European Regional Development Fund and the Walloon Region) are thanked for their support.

References

[1] Caravan P 2006 Strategies for increasing the sensitivity gadolinium based MRI contrast agents *Chem. Soc. Rev.* **35** 512–23

[2] Merbach A, Helm L and Toth E 2013 *The Chemistry of Contrast Agents in Medical Magnetic Resonance Imaging* 2nd edn (Chichester: Wiley and Sons)

[3] Aime S and Caravan P 2009 Biodistribution of gadolinium-based contrast agents, including gadolinium deposition *J. Magn. Reson. Imaging* **30** 1259–67

[4] Idée J M, Port M, Medina C, Lancelot E, Fayoux E, Ballet S and Corot C 2008 Possible involvement of gadolinium chelates in the pathophysiology of nephrogenic systemic fibrosis: a critical review *Toxicology* **248** 77–88

[5] Delli-Castelli D, Gianolio E, Genimatti-Crich S, Terreno E and Aime S 2008 Metal containing nanosized systems for MR-Molecular Imaging applications *Coord. Chem. Rev.* **252** 2424–43

[6] Huang C H and Tsourkas A 2013 Gd-based macromolecules and nanoparticles as magnetic resonance contrast agents for molecular imaging *Curr. Top. Med. Chem.* **13** 411–21

[7] Cormode D P, Jarzyna P A, Mulder W J M and Fayad Z A 2010 Modified natural nanoparticles as contrast agents for medical imaging *Adv. Drug Del. Rev.* **62** 329–38

[8] Aime S, Frullano L and Genimatti-Crich S 2002 Compartmentalization of a gadolinium complex in the apoferritin cavity: a route to obtain high relaxivity contrast agents for magnetic resonance imaging *Angew. Chem. Int. Ed.* **41** 1017–9

[9] Accardoa A, Tesauroa D, Alojb L, Pedonea C and Morelli G 2009 Supramolecular aggregates containing lipophilic Gd (III) complexes as contrast agents in MRI *Coord. Chem. Rev.* **253** 2193–213

[10] Della-Rocca J and Lin W 2010 Nanoscale metal-organic frameworks: magnetic resonance imaging contrast agents and beyond *Eur. J. Inorg. Chem.* **24** 3725–34

[11] Ghiassi K B, Olmstead M M and Balch A L 2014 Gadolinium-containing endohedral fullerenes: structure and function as magnetic resonance imaging (MRI) agents *Dalton Trans.* **43** 7346–58

[12] Na H B, Song I C and Hyeon T 2009 Inorganic nanoparticles for MRI contrast agents *Adv. Mater.* **21** 2133–48

[13] Soleimani A, Martinez F, Economopoulos V, Foster P J, Scholl T J and Gillies E R 2013 Polymer cross-linking: a nanogel approach to enhancing the relaxivity of MRI contrast agents *J. Mater. Chem.* B **1** 1027–34

[14] Lux J, Chan M, Vander Elst L, Schopf E, Mahmoud E, Laurent S and Almutairi A 2013 Metal chelating crosslinkers form nanogel with high chelation stability *J. Mater. Chem.* B **1** 6359–64

[15] Chen Z, Yu D, Liu C, Yang X, Zhang N, Ma C, Song J and Lu Z 2011 Gadolinium-conjugated PLA-PEG nanoparticles as liver targeted molecular MRI contrast agent *J. Drug Target* **19** 657–65

[16] Ishihara T, Kubota T, Choi T, Takahashi M, Ayano E, Kanazawa H and Higaki M 2009 Polymeric nanoparticles encapsulating betamethasone phosphate with different release profiles and stealthiness *Int. J. Pharm.* **375** 148–54

[17] Jain R A 2000 The manufacturing techniques of various drug loaded biodegradable poly(lactide-*co*-glycolide) (PLGA) devices *Biomaterials* **21** 2475–90

[18] Peltonen L, Aitta J, Hyvönen S, Karjalainen M and Hirvonen J 2004 Improved entrapment efficiency of hydrophilic drug substance during nanoprecipitation of poly(l)lactide nanoparticles *AAPS Pharmaceut. Sci. Technol.* **5** 115–6

[19] Raghunand N, Guntle G P, Gokhale V, Nichol G S, Mash E A and Jagadish B 2010 Design, synthesis, and evaluation of 1,4,7,10-tetraazacyclododecane-1,4,7-triacetic acid derived, redox-sensitive contrast agents for magnetic resonance imaging *J. Med. Chem.* **53** 6747–57

[20] Fessi H, Puisieux F, Devissaguet J P, Ammoury N and Benita S 1989 Nanocapsule formation by interfacial polymer deposition following solvent displacement *Int. J. Pharm.* **55** R1–4

[21] Courant T *et al* 2012 Hydrogels incorporating GdDOTA: towards highly efficient dual T_1/T_2 MRI contrast agents *Angew. Chem.* **124** 9253–6

[22] Mosmann T 1983 Rapid colorimetric essay for cellular growth and survival: application to proliferation and cytotoxicity assays *J. Immunol. Methods* **65** 55–63

[23] Callewaert M, Dukic S, Van-Gulick L, Vittier M, Gafa V, Andry M C, Molinari M and Roullin V G 2012 Etoposide encapsulation in surface-modified poly(lactide-co-glycolide) nanoparticles strongly enhances glioma antitumor efficiency *J. Biomed. Mater. Res.* A **101A** 1319–27

[24] Bœuf G *et al* 2014 Encapsulated ruthenium(II) complexes in biocompatible poly(D,L-lactide-co-glycolide) nanoparticles for application in photodynamic therapy *ChemPlusChem.* **79** 171–80

[25] Nieddu M, Rassu G, Boatto G, Bosi P, Trevisi P, Giunchedi P, Carta A and Gavinin E 2014 Improvement of thymol properties by complexation with cyclodextrins: *In vitro* and *in vivo* studies *Carbohydr. Polym.* **102** 393–9

[26] Rowe R C, Sheskey P J, Cook W G and Fenton M E (ed) 2012 *Handbook of Pharmaceutical Excipients* 7th edn (London: Pharmaceutical Press)

[27] Ridhurkar D N, Akhter-Ansari K, Kumar D, Kaul N S, Krishnamurthy T, Dhawan S and Pillai R 2013 Inclusion complex of a prepitant with cyclodextrin: evaluation of physico-chemical and pharmacokinetic properties *Drug Dev. Ind. Pharm.* **39** 1783–92

[28] Brigger I, Dubernet C and Couvreur P 2002 Nanoparticles in cancer therapy and diagnosis *Adv. Drug. Deliv. Rev.* **54** 631–51

[29] Cho W S, Thielbeer F, Duffin R, Johansson E M V, Megson I L, MacNee W, Bradley M and Donaldson K 2014 Surface functionalization affects the zeta potential coronal stability and membranolytic activity of polymeric nanoparticles *Nanotoxicology* **8** 202–11

[30] Courant T, Roullin V G, Cadiou C, Delavoie F, Molinari M, Andry M C, Gafa V and Chuburu F 2010 Vectorization of copper complexes via biocompatible and biodegradable PLGA nanoparticles *Nanotechnology* **21** 165101–8

[31] Oyarzun-Ampuero F A, Brea J, Loza M I, Torres D and Alonso M J 2009 Chitosan-hyaluronic acid nanoparticles loaded with heparin for the treatment of asthma *Int. J. Pharm.* **381** 122–9

[32] Sah H, Thoma L A, Desu H R, Sah E and Wood G C 2013 Concepts and practices used to develop functional PLGA-based nanoparticulate systems *Int. J. Nanomedicine* **8** 747–65

[33] Li M, Panagi Z, Avgoustakis K and Reineke J 2012 Physiologically based pharmacokinetic modeling of PLGA nanoparticles with varied mPEG content *Int. J. Nanomedicine* **7** 1345–56

[34] Courant T *et al* 2013 Biocompatible nanoparticles and gadolinium complexes for MRI applications *C. R. Chim.* **16** 531–9

[35] Ratzinger G, Agrawal P, Körner W, Lonkai J, Sanders H M H S, Terreno E, Wirth M, Strijkers G J, Nicolay K and Gabor F 2010 Surface modification of PLGA nanospheres with Gd-DTPA and Gd-DOTA for high-relaxivity MRI contrast agent *Biomaterials* **31** 8716–23

[36] Zhang Y, Zhou J, Guo D, Ao M, Zheng Y and Wang Z 2013 Preparation and characterization of gadolinium-loaded PLGA particles surface modified with RGDS for the detection of thrombus *Int. J. Nanomedicine* **8** 3745–56

[37] Ichikawa H *et al* 2013 Gadolinium-loaded chitosan nanoparticles for neutron-capture therapy: influence of micrometric properties of the nanoparticles on tumor-killing effect *Appl. Radiat. Isot.* **88** 109–13

[38] Othman M *et al* 2011 Synthesis and physicochemical characterization of new squalenoyl amphiphilic gadolinium complexes as nanoparticle contrast agents *Org. Biomol. Chem.* **9** 4367–86

[39] Zhang L, Liu Y, Yu D and Zhang N 2013 Gadolinium-loaded chitosan nanoparticles as magnetic resonance imaging contrast agent for the diagnosis of tumor *J. Biomed Nanotechnol.* **9** 863–9

[40] Avgoustakis K, Beletsi A, Panagi Z, Klepetsanis P, Karydas A G and Ithakissios D S 2002 PLGA-mPEG nanoparticles of cisplatin: *in vitro* nanoparticle degradation, *in vitro* drug release and *in vivo* drug residence in blood properties *J. Control Release* **79** 123–35

[41] Wu L, Zhang J and Watanabe W 2011 Physical and chemical stability of drug nanoparticles *Adv. Drug Deliv. Rev.* **63** 456–69

[42] Dufort S, Sancey L and Coll J L 2012 Physico-chemical parameters that govern nanoparticles fate also dictate rules for their molecular evolution *Adv. Drug Deliv. Rev.* **67** 179–89

[43] Szekeres M, Toth I Y, Illés E, Hajdu A, Zupko I, Farkas K, Oszlanczi G, Tiszlavicz L and Tombacz E 2013 Chemical and colloidal stability of carboxylated core–shell magnetite nanoparticles designed for biomedical applications *Int. J. Mol. Sci.* **14** 14550–74

[44] Sadrieh N 2006 FDA Considerations For Regulation Of Nanomaterial Containing Products *FDA Docket* # 2006-4241B1-02-31

[45] Zweers M L T, Engbers G H M, Grijpma D W and Feijen J 2004 *In vitro* degradation of nanoparticles prepared from polymers based on DL-lactide, glycolide and poly(ethylene oxide) *J. Control Release* **100** 347–56

[46] Rojnik M *et al* 2012 *In vitro* and *in vivo* characterization of temoporfin-loaded PEGylated PLGA nanoparticles for use in photodynamic therapy *Nanomedicine* **7** 663–77

[47] Thakur R, Das A and Chkraborty A 2014 The fate of anticancer drug, ellipticine in DPPC and DMPC liposomes upon interaction with HSA: a photophysical approach *J. Photochem. Photobiol.* **130** 122–31

[48] Kumar G, Sharma S, Shafiq N, Khuller G K and Malhotra S 2012 Optimization, *in vitro-in vivo* evaluation, and short-term tolerability of novel levofloxacin-loaded PLGA nanoparticle formulation *J. Pharm. Sci.* **101** 2165–76

[49] Musumeci T, Ventura C A, Giannone I, Ruozi B, Montenegro L, Pignatello R and Puglisi G 2006 PLA/PLGA nanoparticles for sustained release of docetaxel *Int. J. Pharm.* **325** 172–9

[50] Lewinski N, Colvin V and Drezek R 2008 Cytotoxicity of nanoparticles *Small* **4** 26–49

[51] Taki T, Ohnishi T, Arita N, Hiraga S and Hayakawa T 1998 *In vivo* etoposide-resistant C6 glioma cell line: significance of altered DNA topoisomerase II activity in multi-drug resistance *J. Neurooncol.* **36** 41–53

[52] Bayreuther K, Francz P I, Gogol J, Hapke C, Maier M and Meinrath H G 1991 Differentiation of primary and secondary fibroblasts in cell culture systems *Mutation Research/DNAging* **256** 233–42

[53] Stella V J and He Q 2008 *Cyclodextrins Toxicologic Pathology.* **36** 30–42

[54] Nicolle G M, Toth E, Eisenwiener K-P, Macke H R and Merbach A E 2002 From monomers to micelles: investigation of the parameters influencing proton relaxivity *J. Biol. Inorg. Chem.* **7** 757–69

[55] Aime S, Botta M, Fedeli F, Gianolio E, Terreno E and Anelli P 2001 High-relaxivity contrast agents for magnetic resonance imaging base on multisite interactions between a β-cyclodextrin oligomer and suitably functionalized Gd^{III} chelates *Chem. Eur. J.* **7** 5262–9

[56] Alric C *et al* 2008 Gadolinium chelate coated gold nanoparticles as contrast agents for both x-ray computed tomography and magnetic resonance imaging *J. Am. Chem. Soc.* **130** 5908–15

[57] New K, Huang C H and Tsourkas A 2013 Gd-labeled glycol chitosan as a pH-responsive magnetic resonance imaging agent for detecting acidic tumor microenvironments *J. Med. Chem.* **56** 7862–9